Adsorption of Charged Block Copolymers: Effect on Colloidal Stability

R. Israëls, F. A. M. Leermakers,* and G. J. Fleer

Department of Physical and Colloid Chemistry, Wageningen Agricultural University, Dreijenplein 6, 6703 HB Wageningen, The Netherlands

Received March 10, 1994; Revised Manuscript Received October 7, 1994[⊗]

ABSTRACT: We study the effect on colloidal stability of the adsorption of diblock copolymers with a charged buoy block. Using a scaling as well as an SCF approach, we focus on the high-charge regime and find that adsorbed amounts are very low. Nevertheless, the adsorbed polymer causes a significant repulsive interaction between two surfaces. For low charges and long anchor blocks ("anchor-dominated regime") the colloidal stability would be expected to rise with increasing charge on the buoy block. In our high-charge regime we find the reverse; i.e., the electrosteric repulsive interaction increases with increasing salt concentration and decreasing buoy length or buoy charge. This counterintuitive behavior is caused by the effect of the electrostatic interactions on the adsorbed amount: stronger interactions lead to a lower adsorbed amount, which in turn leads to a weaker repulsion. Numerical SCF calculations confirm these scaling predictions.

I. Introduction

It is now well established that homopolymers can induce attractive as well as repulsive interactions in colloidal suspensions. Colloidal stability may be enhanced when thick adsorbed layers give rise to steric repulsion forces. On the other hand, attraction is found when a chain can adsorb simultaneously onto two or more particles, thereby forming so-called bridges. Different situations may be distinguished. If the two surfaces are only partially covered, bridges are easily formed and the interaction is attractive. When the colloidal particles are fully covered by polymer, flocculation may occur if chains can desorb quickly enough. However, polymer desorption is often extremely slow. In most cases the polymers are essentially irreversibly adsorbed to the surface and the interaction is repulsive.

In the remainder of the text we will refer to the fast desorption as a "free" system: the polymer is free to leave the gap between the particles. The slow desorption will be referred to as a "restricted" system: the polymers are *not* allowed to exit from the gap.

Because of the possibility of bridge formation, homopolymer adsorption is not expected to be the optimal way to stabilize colloidal systems. An obvious way to improve the stabilizing capacity of a polymer is to graft the chains chemically onto the surface. In this way high adsorbed amounts can be achieved, while desorption is completely prevented. If a nonadsorbing polymer is end-grafted and the grafting density is high enough, a so-called brush is formed. Such a brush could be very effective in stabilizing suspensions: bridging is impossible. The interaction between two brushes is often described by the Alexander−de Gennes theory.[1−3] If the separation M between the particles is smaller than twice the thickness H of an isolated brush, the repulsive pressure $P(M)$ scales as

$$P(M) \approx \frac{kT}{\sigma^{3/2}}\left[\left(\frac{2H}{M}\right)^{9/4} - \left(\frac{M}{2H}\right)^{3/4}\right] \qquad (1)$$

where σ is the grafting density and kT the thermal energy. The first term within the brackets gives the osmotic repulsion between the brush molecules, whereas the second term represents the gain in elastic energy when the brush is compressed. For $M/2H$ in the range 0.2−0.8, the above expression is roughly exponential: $P(M) \sim e^{-cM/H}$, where c is a constant.

Another class of promising stabilizers is formed by A_xB_y diblock copolymers of which the anchor block A adsorbs to the surface and the buoy block B extends into the solution. If the anchor is strong, desorption is virtually impossible and the properties of the adsorbed layer are similar to those of a brush of B segments. It was shown by Evers et al.[4] that such an A_xB_y diblock copolymer can prevent flocculation also when the adsorbed molecules are in full equilibrium with dissolved ones (a free system).

In the above only short-range interactions were considered. In water-based systems, however, also long-range electrostatic interactions generally play an important role. There are two reasons to study water-based systems. First, for environmental reasons, in many commercial products organic solvents will have to be substituted by water in the near future. Second, this class of systems is relevant in a biological context, where colloidal stability is an important issue.

Recently, there has been considerable theoretical progress on the charged counterparts of the two systems mentioned above: brushes and diblock copolymer adsorption.

In a paper by Pincus,[5] which was followed by a series of papers by Zhulina et al.,[6−11] the structure of charged brushes was analyzed. Depending on the salt concentration ϕ_s, on the average charge α per segment, and on the anchoring density σ, at least three brush regimes may be distinguished. We may summarize the results as follows: at high ϕ_s electrostatic interactions are fully screened and the brush behaves as a neutral one, with a parabolic density profile. At low ϕ_s electrostatic interactions dominate: the profile changes from a parabola to a Gaussian and the thickness becomes independent of the grafting density. This regime has been called the osmotic brush regime. At intermediate ϕ_s, the salted brush regime may be found, in which external salt penetrates into the brush; the profile is still parabolic and the electrostatic interactions can be incorporated into an effective excluded volume parameter:

[⊗] Abstract published in *Advance ACS Abstracts,* January 15, 1995.

0024-9297/95/2228-1626$09.00/0

$$v_{eff} = v + \alpha^2/\phi_s \quad (2)$$

where v is the excluded volume parameter of the uncharged segments. The brush thickness H is given by

$$H \sim N(v_{eff}\sigma)^{1/3} \quad (3)$$

which is analogous to the scaling properties of uncharged brushes as given by Alexander and de Gennes[1-3] and Milner, Witten, and Cates.[12]

The adsorption of ionic diblock copolymers, A_xB_y molecules of which the buoy block B carries a charge, is the main subject of the present contribution. Only very recently, three theoretical studies of this system were published. A first route was followed independently by two groups,[13,14] who combined the results of Pincus on charged brushes[5] with those of Marques, Joanny, and Leibler[15] on uncharged diblock copolymers adsorbing from a selective solvent. They find a regime which we will refer to as the selective solvent (SS) regime, where the ionic diblock adsorbs in relatively high amounts. The A segments, being exposed to a nonsolvent, are supposed to form a molten layer at the surface, whereas a charged brush is formed by the B segments. A central result, as put forth by Wittmer et al.,[14] is that the SS regime can only be found for not too highly charged B blocks. Specifically, if the following requirement

$$\alpha < N_A^{4/5} N_B^{-6/5} (\gamma_A)^{6/5} \left(\frac{l_B}{d}\right)^{2/5} \quad (4)$$

is not fulfilled, the adsorbed amount is expected to be very low. In (4), α is again the average charge per B segment, N_A and N_B are the respective block lengths, d is the size of one segment, l_B is the Bjerrum length (which roughly equals 7 Å in water), and γ_A gives the free energy (expressed in units of kT per area d^2) of an interface between A and solvent segments.

We followed an alternative route to analyze ionic block copolymer adsorption[16] and combined the model developed by Evers et al.[17] for the adsorption of uncharged diblock copolymers with the polyelectrolyte adsorption model of Böhmer et al.[18] We studied adsorption from a nonselective solvent and concluded that low adsorbed amounts are to be expected for a wide range of parameters. At low salt concentration or high charge density ($\alpha^2/\phi_s \gg v$), electrostatic interactions dominate the scaling behavior, and the adsorbed amounts are very low indeed, below the detection limit of conventional methods. Our results are different from those of Argillier et al.[13] or Wittmer et al.,[14] but there is no contradiction: we chose our parameters in such a way that electrostatic interactions can be expected to be important and found low adsorbed amounts; they chose to describe a regime with high adsorbed amounts and concluded that it exists only when electrostatic interactions are not too strong. In order to provide a link between the two cases, we will give one typical example of a system in the SS regime (Figure 2).

The main goal of the paper, however, is to investigate and prove the relevance of the low-coverage (LC) regime. As stated by Wittmer et al., the extremely low adsorbed amounts in this regime should, in principle, preclude a big effect on stability. We will evaluate this expectation quantitatively and calculate the interaction between two surfaces covered with ionic diblock copolymers. Specifically, we investigate the effect of N_A, N_B, α, and ϕ_s on the magnitude of the interaction and on the shape of the interaction curve.

The remaining part of this paper is organized as follows. In section II we describe the SCF model, and in section III we derive an analytical expression for the force profile. We represent results from the SCF model in section IV. The main conclusions are discussed in section V.

II. SCF Model

In the following we summarize the main points of our theory. The self-consistent-field (SCF) theory rests on four approximations: (I) The space between two flat interfaces (representing colloidal particles) is discretized using a lattice, which serves as a system of coordinates on which segments and solvent molecules are positioned. The lattice cells are organized in flat layers of homogeneous density, containing L lattice sites each. The layers are numbered $z = 1, ..., M$. Layers 0 and $M + 1$ are occupied by the solid substrate S; so effectively we model the interaction between particles which are large with respect to the polymer layer thickness. (II) Chain conformations are generated with a first-order Markov approximation, equivalent to a freely jointed chain model. (III) The many-chain problem is reduced to that of a test chain in an external potential field generated by all the chains in the system. The potential field is a function of the z coordinate only, which implies a meanfield approximation within each lattice layer. Thus, lateral inhomogeneities are not considered. Potential gradients in the z direction cause segment densities to be only a function of z coordinates as well. In this sense one can refer to this version of the SCF theory as a one-dimensional theory which, however, models a three-dimensional system. (IV) The system is assumed to be incompressible, which means that each layer is exactly filled by segments, solvent, or ion species: no vacancies are allowed. Below we will give a concise elaboration of these four points. For a full derivation of the model, as well as a discussion of its approximations, we refer to a recent review by Fleer et al.[19]

In the lattice theory, molecular details on length scales smaller than monomers are neglected. All segment types are taken to be of equal size. They are indicated by the subscript A, B, ..., representing anchor block segments, buoy block segments, water molecules, positively or negatively charged ions, and adsorbent segments. Molecules are indicated by the subscript i, j, ... Polymeric molecules may consist of several segment types; the ranking number of their segments is $s = 1, 2, ..., N_i$, where N_i is the chain length of component i. Their composition is very important; in this paper we discuss diblock copolymers A_xB_y where segments $s = 1, ..., x$ are of type A (anchor) and segments $s = x + 1, ..., N$ are of type B (buoy).

In a Markov approximation the segment density is found by

$$\phi_i(z,s) = C_i \frac{G_i(z,s|1)\, G_i(z,s|N)}{G_i(z,s)} \quad (5)$$

Here $G_i(z,s|1)$ is the statistical weight to find in layer z the end segment of a sequence of s segments, of which the composition is dictated by the molecular architecture of component i. Analogously, the quantity $G_i(z,s|N)$ is defined as the overall statistical weight for the chain

part $s' = N, N-1, ..., s$ to be in the system with the only constraint that segment s, the end point of this sequence, is in layer z. In the composition law (eq 5) a correction for the double counting of segment s is included by the division by the free segment distribution function $G_i(z,s)$.

The normalization constant C_i is, for molecules which are in equilibrium with the bulk solution, given by $C_i = \phi_i^b/N_i$, where the bulk concentration ϕ_i^b is an input quantity. For a restricted equilibrium, when the number of molecules between the surfaces is fixed, C_i follows from the condition $\sigma_i = \sum_z \phi_i(z,s)$; now σ_i is the input quantity. Defining $G_i(1|N)$ as the overall statistical weight to find a chain i in the system, according to $G_i(1|N) = \sum_z G_i(z,1|N)$, we find $C_i = \sigma_i/[G_i(1|N)]$.

The chain end distribution functions follow from a recurrence type relation which is a discrete version of the Edwards diffusion equation:

$$G_i(z,s|1) = \langle G_i(z,s-1|1)\rangle\, G_i(z,s) \tag{6}$$

and

$$G_i(z,s|N) = \langle G_i(z,s+1|N)\rangle\, G_i(z,s) \tag{7}$$

where the angular brackets indicate an averaging over the neighbors of a site in layer z. For a cubic lattice, such an average is defined by

$$\langle f(z)\rangle = \frac{f(z-1) + 4f(z) + f(z+1)}{6} \tag{8}$$

The function $f(z)$ may be any function, such as a chain end distribution function or a volume fraction.

In eqs 5–7 the free segment distribution function $G_i(z,s)$ is a central quantity. It is defined as the Boltzmann factor of the local segment potential. When segment s of molecule i is of type A, then $G_i(z,s) = G_A(z) = \exp(-u_A(z))$. The dimensionless potential $u_A(z)$ is expressed in units of kT, as we will do for all potentials and energies from here on. Thus, eq 5 can be evaluated once the segment potentials are known. The key ingredient of an SCF theory is that the potentials themselves are again a function of the local densities. In this paper we include three terms in the local potential:

$$u_A(z) = u'(z) + u_A^{mix}(z) + u_A^{el}(z) \tag{9}$$

The first term originates from the incompressibility constraint and is in fact a Lagrange parameter. The second term accounts for short-range interactions:

$$u_A^{mix}(z) = \sum_B \chi_{AB}\,(\langle\phi_B(z)\rangle - \phi_B^b) \tag{10}$$

The third term in eq 9 represents the long-range electrostatic interactions:

$$u_A^{el}(z) = \alpha_A y(z) \tag{11}$$

In eq 10 the summation index B runs over all segment types in the system, including the segments of the adsorbent. The parameter χ_{AB} is the familiar Flory–Huggins interaction parameter, defined as the free energy associated with the process of transferring an A segment from an A environment to a B environment. In eq 11, α_A represents the valency of the segment type A, and $y(z)$ is the dimensionless electrostatic potential, in units of kT per elementary charge e. The reference point of the potentials (including $y(z)$) is the bulk solution. This results in a free segment distribution function $G_A(z) = 1$ in the bulk, which implies ideal chain statistics in this part of the system. The use of a homogeneous bulk system that is in equilibrium with the inhomogeneous interface is the usual mean-field ansatz. We explicitly assume that there is no structure formation in the bulk, which would be a severe approximation for the SS regime, where micelle formation is to be expected. Such a system can be modeled in an SCF approach by simultaneously considering the equilibrium between polymer molecules in the adsorption layer and those in micelles.[20,21] As stated before, we consider mainly nonselective solvents, for which these complications play no role.

The evaluation of the local electrostatic potential, under the constraint that the system is electroneutral, can conveniently be performed in each layer once the effective charge density $\varrho(z)$ and the local dielectric permittivity are known. Both quantities are computed from the segment distributions. Obviously, the charge density can be calculated as $\varrho(z) = (e/d^2)\sum_A \alpha_A \phi_A(z)$, where e is the elementary charge, and d the lattice spacing. We approximate the dielectric permittivity in a layer by the mean-field expression $\epsilon(z) = \sum_A \epsilon_A \phi_A(z)$.

Gauss' law couples the charge distribution to the distribution of electrostatic potentials. It states generally that the integral of the field strength E across a closed area surrounding a given volume equals the ratio of the charge and the dielectric permittivity in this volume. In the present case, we take layer z as this volume and write E as $-(kT/ed)\partial y/\partial z$, where the lattice spacing d is needed to convert the dimensionless distance z into a real distance. If ϵ is taken to be a constant, the discrete version of Gauss' law becomes

$$\frac{y(z) - y(z-1)}{d} + \frac{y(z) - y(z+1)}{d} = \frac{e}{kT}\frac{\varrho(z)}{\epsilon} \tag{12}$$

This equation can also be written as $C\{y(z) - y(z-1) + y(z) - y(z+1)\} = e\varrho(z)/kT$, where $C = \epsilon/d$ is the capacitance per unit area. If $C(z) = \epsilon(z)/d$ is a function of z, we have to modify this expression, taking into account that ϵ changes discontinuously halfway the charge planes. The average capacitance $C(z,z')$ between neighboring planes z and z' is given by

$$C^{-1}(z,z') = \frac{1}{2}\{C^{-1}(z) + C^{-1}(z')\} \tag{13}$$

The corrected version of eq 12 is now

$$C(z,z-1)\{y(z) - y(z-1)\} + C(z,z+1)\{y(z) - y(z+1)\} = \frac{e\varrho(z)}{kT} \tag{14}$$

It is easily seen that eq 14 reduces to eq 12 if C is constant.

The electroneutrality of the system is ensured by setting the field strength at the boundaries to zero:

$$\left.\frac{\partial y}{\partial z}\right|_{z=0} = \left.\frac{\partial y}{\partial z}\right|_{z=M} = 0 \tag{15}$$

We use a discrete version, analogous to eq 14.

All told, the set of equations (5–15) can be solved numerically. The SCF solution is characterized by the fact that the set of local potentials $\{u_A(z)\}$ (eqs 9–11)

must be consistent with $\{\phi_A(z)\}$ (eq 5). The solution is only accepted when the incompressibility constraint is obeyed. This solution is routinely obtained numerically; analytical solutions can, in general, not be found.

We now turn our attention to the evaluation of the free energy of interaction between two interfaces. As explained in the Introduction, we distinguish full and restricted equilibrium. These two situations are controlled by the choice for C_i, as discussed below eq 5. The free energy of the system (in units of kT per lattice site) at an interplate separation M is given by

$$A(M) = \sum_i \sigma_i \ln(N_i C_i) - \sum_{z,A} \phi_A(z) \ln G_A(z) + U^{mix} + U^{el} \quad (16)$$

In eq 16 the last two terms represent the energetic contributions to the free energy: U^{mix} is the contact energy and U^{el} the electrostatic energy. These terms are given by

$$U^{mix} = U^* + \frac{1}{2} \sum_{z,A,B} \chi_{AB} \langle \phi_A(z) \rangle \phi_B(z) \quad (17)$$

and

$$U^{el} = \sum_z \frac{1}{2} \varrho(z)\, y(z) \quad (18)$$

The quantity U^* is the mixing energy in a suitable reference state which we take here as the pure amorphous phase of each individual component. This reference state is not important for calculating the interaction free energy. The Flory–Huggins parameter χ_{AB} is the mixing energy per A–B contact.

Free molecules are in full equilibrium with the bulk solution: their chemical potential equals the chemical potential of molecules in the bulk solution:[17]

$$\mu_j = \ln \phi_j^b + 1 - N_j \sum_i \frac{\phi_i^b}{N_i} + \frac{1}{2} N_j \sum_{A,B} \chi_{AB} (\phi_{Aj}^* - \phi_A^b)(\phi_B^b - \phi_{Bj}^*) \quad (19)$$

where ϕ_{Aj}^* is the volume fraction of segments A in the reference state of pure component j. We define the excess free energy $A^\sigma(M)$ as

$$A^\sigma(M) = A(M) - \sum_i{}' \sigma_i \mu_i \quad (20)$$

where the prime indicates that the summation runs over the free components only. The interaction free energy at separation M is the difference between the excess free energy (as calculated from eq 20) at separation M and that at infinite separation:

$$A^{int}(M) = A^\sigma(M) - A^\sigma(\infty) \quad (21)$$

In the actual calculations this "infinite separation" is taken to be finite, but large enough so that it does not affect the results as found by eq 21.

III. Scaling

As shown before,[16] the adsorbed amount and layer thickness in the low-coverage (LC) regime can be interpreted in terms of a simple analytical model: the total free energy of the system can be approximated by a summation of elastic, osmotic, and adsorption free energy contributions. We use the Gaussian approximation for the elastic free energy, which gives $\sigma H^2/N_B$. The osmotic contribution is the same as that for charged brushes in the salted brush regime, resulting in a contribution $v_{eff}\sigma^2 N_B^2/H$. Furthermore, it is assumed that the A block is adsorbed in a flat conformation, so that the adsorption energy is proportional to $N_A\sigma$. Hence,

$$A = \frac{\sigma H^2}{N_B} + \frac{v_{eff}\sigma^2 N_B^2}{H} - N_A\sigma \quad (22)$$

Note that the translational entropy for the adsorbed molecules is neglected. Disregarding the effects of interactions in the bulk, we set the partial derivatives $\partial A/\partial\sigma$ and $\partial A/\partial H$ to zero. This immediately leads to

$$\sigma \sim (N_A/N_B)^{3/2} (v_{eff})^{-1} \quad (23)$$

and

$$H \sim (N_A N_B)^{1/2} \quad (24)$$

These results were obtained already in a previous publication.[16] We now continue and derive expressions for the repulsive force between two of these adsorbed layers. If we ignore interpenetration of the two brushes, the energetic effect of squeezing the brush for $0 < M < 2H$ is simply obtained by inserting $H = M/2$ in eq 22. We assume restricted equilibrium and take σ to remain constant, given by eq 23. Furthermore, we omit the adsorption energy term, which is constant anyway, and the elastic contribution since it becomes negligible compared to the rapidly increasing osmotic pressure. The interaction sets in when the outer parts of the brushes meet, i.e., at $M = 2H$. Defining the interaction with respect to this point, the interaction energy A^{int} is found as

$$A^{int}(M) \approx \frac{N_A^3}{N_B} (v_{eff})^{-1} (1/M - 1/2H) \qquad [0 < M < 2H] \quad (25)$$

This expression approaches infinity when M goes to zero. The central part of a curve $A(M)$ vs M is again roughly exponential: if $A(M)$ is plotted on a log–lin scale, we find a straight part. The slope of this exponential part is affected only by the last factor within brackets; it is inversely proportional to the brush thickness H. The prefactor $N_A^3/(N_B v_{eff})$ determines the offset of the line and is a measure for colloidal stability.

IV. Results and Discussion

Parameters. In the calculations we use a cubic lattice, with lattice spacing $d = 0.6$ nm, leading to a number concentration of lattice sites equal to $(0.6 \times 10^{-9})^{-3}$ m^{-3}, or a molar concentration of 7.7 mol/L. This value is important, since it provides the conversion factor from a volume fraction to a molarity. As explained in the Introduction, we consider mainly the low coverage–high charge (LC) regime, in which the solvency has very little effect on the adsorption behavior. As before,[16] we choose Θ conditions for both segment types in the polymer: $\chi_{AO} = \chi_{BO} = 0.5$, where O refers to the solvent. Furthermore, the uncharged A segments

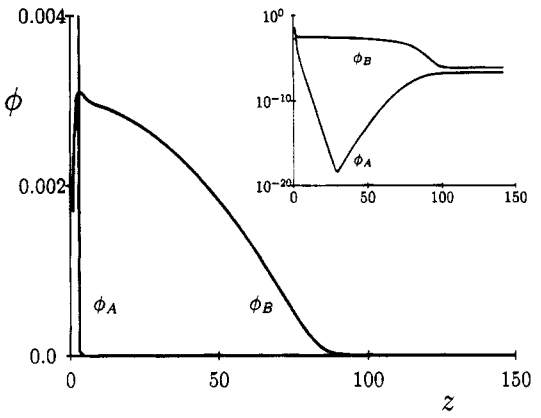

Figure 1. Volume fraction profiles of adsorbing A segments and buoy B segments in the LC regime: low coverage–high charge. The curves are plotted on a lin–lin as well as on a log–lin (inset) scale. Parameters: $N_A = 100$, $N_B = 400$, $\phi_s = 10^{-2}$, $\phi_p = 10^{-6}$, $\alpha_B = 1.0$, $\chi_{AO} = \chi_{BO} = 0.5$, $\chi_s = 1$, cubic lattice with $d = 0.6$ nm at a separation $M = 300$ layers.

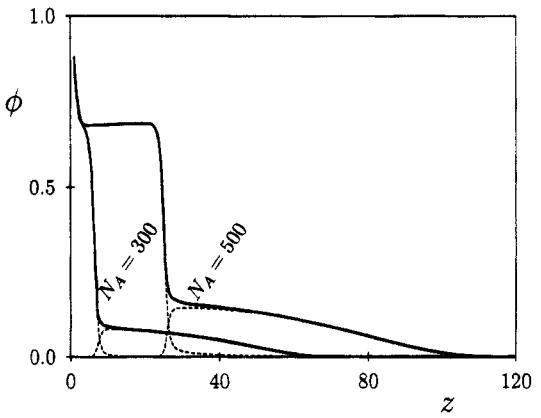

Figure 2. Volume fraction profiles in the charged brush regime of diblock copolymers $A_{300}B_{200}$ and $A_{500}B_{200}$ (solid curves) and the individual contributions of A and B segments (dashed curves). Parameters: $\chi_{AO} = 1.0$, $\chi_{BO} = 0.0$, $\alpha_B = 0.2$, $\phi_s = 0.01$, other parameters as in Figure 1.

adsorb to the surface with an adsorption energy of 1 kT per segment ($\chi_s = 1$), whereas the B segments of the buoy block have no affinity for the surface. The charge of the B segments is expressed through α, the average valence of one B segment. In this way the charges on the chain are smeared out: we model a chain of which every tenth B segment is charged as a chain in which each segment has a charge of 0.1 e. The relative dielectric constant of the solvent is set to 80, and that of all other species equals 5. In the one example we give for the selective solvent (SS) regime (Figure 2), χ_{AO} is chosen as 1.0 (nonsolvent) and χ_{BO} as 0 (good solvent).

Volume Fraction Profiles. Before turning to the main section of our results, i.e., the description of force curves in the LC regime, we briefly review the characteristics of the adsorbed layer in this regime (Figure 1). As a comparison, we also present an example of volume fraction profiles for the SS regime (Figure 2).

In Figure 1 typical volume fraction profiles in the LC regime are presented for anchoring A and buoy block B segments. The inset shows the same profiles on a logarithmic scale for ϕ. As discussed before,[16] the most prominent features of these profiles are the following: (I) There is an almost absolute confinement of A segments to the first layer in contact with the surface. The concentration in this layer, $\phi_A(1) = 0.038$, is outside the range plotted in Figure 1. (II) The "brush" region composed of B segments is extremely dilute. The density in this region is below the brush limit for *uncharged* molecules, which is defined as the density above which B blocks start to overlap physically. (III) However, the density is obviously high enough to create a charged brush, in which the B tails are highly stretched due to interchain electrostatic interactions.

Recently, it has been shown that lateral inhomogeneities are unimportant in this so-called "salted brush" regime,[11] which extends down to a grafting density $\sigma = \theta/N_B = \alpha^{-2}N_B^{-3}\phi_s^{-1/2}$ if $\phi_s < 1/N_B$, whereas the lower boundary is given by $\sigma = \alpha^{-2}N_B^{-3/2}\phi_s$ for $\phi_s > 1/N_B$. The lateral mean-field approximation, which we adopted in both our numerical and scaling approaches, is valid only in this regime; all our results are calculated for systems for which the brush density is well above these limits.

Profiles of the adsorbed layer in the SS regime are completely different, as shown in Figure 2. These results were obtained by choosing selective solvent conditions for the diblock copolymer and a moderate charge ($\alpha_B = 0.2$) for the segments of the buoy block. Combined with a salt concentration $\phi_s = 10^{-2}$, this leads to rather weak electrostatic interactions. The electrostatic part ($v_{el} = \alpha^2/4\phi_s$) of the total excluded volume interaction $v_{eff} = v + v_{el}$ is then only twice the uncharged contribution $v = 1/2$. The length of the buoy block equals 200, and two different values for the anchor block length were chosen (indicated in the figure). The solid curves in Figure 2 represent the total volume fraction of polymer; in the shape of these curves the individual contributions of the A and B blocks, shown as dashed curves, can easily be recognized.

The general structure of the adsorbed layer in the SS regime is in agreement with the results of Wittmer and Joanny:[14] the anchoring block forms a molten layer of A segments, the density of which is of order unity. Furthermore, the segment density in the B region is clearly high enough to give rise to significant excluded volume interactions. Obviously, since the length of the B block is constant, the area under the B profile is proportional to the number of adsorbed molecules. The figure shows it to *increase* with N_A, which contrasts the results of Wittmer et al. It should be noted, however, that the formation of micelles in the bulk is completely neglected in our present calculation, which precludes a full interpretation of this result.

Interaction Curves in Free and Restricted Equilibrium. In the previous subsection we discussed the structure of the adsorbed layer in two regimes. From now on we focus on the LC regime and study how the adsorbed polymer affects the interaction between two surfaces. We mention again that for the LC system we choose nonselective solvent conditions. This means that in the solution no micelle formation takes place. As explained in the Introduction, we distinguish two different cases. In the "full equilibrium" case the polymer is free to adjust its adsorbed amount during the approach of the two surfaces. Alternatively, in the "restricted equilibrium" we stipulate the amount of polymer between the two surfaces to remain constant.

In Figure 3 we plot the free energy of interaction A^{int} as computed from eq 21 for the same system as in Figure 1, both for full equilibrium (Figure 3a) and for restricted equilibrium (Figure 3b). In both figures, A^{int} is plotted on a linear scale in the main figure; the inset shows the shape of the curves on a log–lin plot.

For restricted and free equilibrium alike, A^{int} increases monotonically with decreasing separation. Thus, the interaction between the adsorbed layers is purely

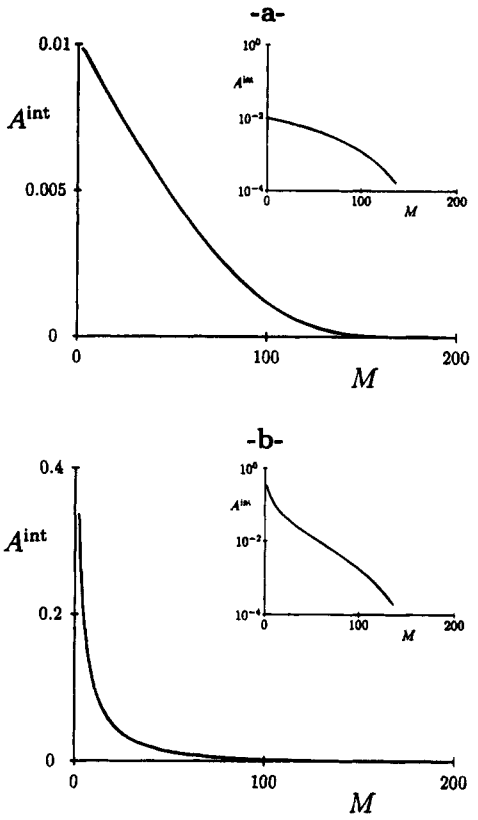

Figure 3. Free energy of interaction A^{int} (in units of kT per lattice site) as a function of plate separation M for full equilibrium (a) and restricted equilibrium (b). The insets show the same data on a logarithmic scale for A^{int}. The parameters for both (a) and (b) are the same as in Figure 1.

repulsive, as expected. Comparing parts a and b of Figure 3, we notice that there is a big difference in the magnitude of the interaction as well as in the shape of the curve.

For the free case depicted in Figure 3a, the repulsive interaction is necessarily lower than for the restricted case in Figure 3b: in any nonequilibrium situation the free energy should be higher than in full equilibrium. For the present system, the two curves are almost identical down to a separation of ~80 layers. Upon a further decrease of M, the two curves diverge, indicating the onset of desorption in the free system. Upon a further decrease of M the repulsive interaction increases nearly linearly in the free system, whereas it increases exponentially (and much stronger) in the restricted case. Thus, the latter follows qualitatively the prediction for the interaction between uncharged brushes by de Gennes (eq 1) or the charged equivalent as given in eq 25. In fact, all our calculations show that the free case leads to a linearly increasing repulsion, whereas for a restricted equilibrium the repulsive interaction increases exponentially. If plotted on a log–lin scale, the two cases may easily be distinguished: only the restricted interaction curve has an inflection point, whereas the slope of the curve representing full equilibrium decreases monotonically with decreasing M.

We believe the restricted case to be the more relevant one for most experimental situations. In order to obtain a more detailed insight in the interaction of two ionic block copolymer layers, we show the volume fraction profiles for three surface separations in Figure 4. In this figure the B profiles of polymer adsorbed on the left-hand-side surface (located at $z = 0$) are plotted as thick curves. The thin mirror images of these curves

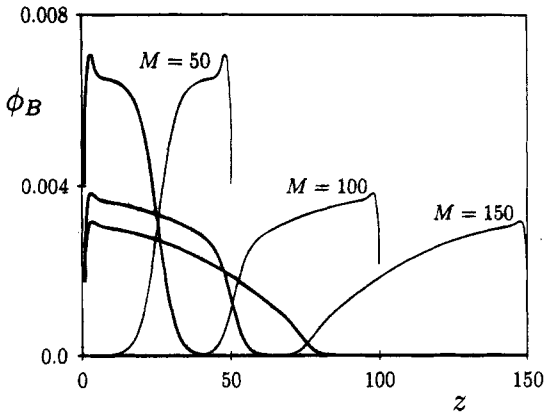

Figure 4. Volume fraction profiles of B segments at different plate separations. Thick curves give the profiles of polymers adsorbed on the left-hand surface. The thin mirror images are the profiles of polymers adsorbed onto surfaces at the indicated separation. Parameters as in Figure 1.

represent the B profiles of polymers adsorbed to the opposite surface, which is located at $M = 50$, 100, and 150, respectively.

From a comparison of Figures 3 and 4 we observe that the repulsive interaction is negligible when the two profiles do not yet overlap, at $M \gtrsim 150$. One might expect that the electrostatic long-range interactions would lead to an onset of repulsion at separations $M > 2H$. Generally, this is expected to be the case when $\kappa^{-1} > H$: when the decay length of the electrostatic potential, i.e., the Debye screening length, is larger than the thickness of the adsorbed layer. Such a regime has been described for anchored brushes.[5] However, in our case $\kappa^{-1} \ll H$ and the repulsion sets in at $M = 2H$, as it would for an uncharged brush. This observation is related to the "local electroneutrality assumption" which applies for charged brushes in the osmotic brush and salted brush regimes:[6,10,11] if the brush thickness is larger than the length scale on which charges are neutralized, the system behaves essentially as an uncharged system. As explained in refs 5, 11, and 22, in this case the electrostatic interactions can be described as resulting from only the translational entropy of counterions. The segment density profile of the latter follows closely the profile of the charged polymer segments.

A further observation we can make from an inspection of Figure 4 is that interpenetration of the chains, although it does take place, is not very prominent. When the two layers are brought in close proximity, they respond by changing their individual conformations, while avoiding mutual interpenetration. This feature has also been described for uncharged brushes.[1-3] It does not imply that the chains would not mix favorably. The correct explanation follows from the fact that chains in an isolated brush are highly stretched (deformed). Compression of the brushes restores the chains to a more natural conformation. This is more favorable than mixing chains of opposite surfaces whereby the chains remain stretched.

The absence of interpenetration is a crucial assumption in the Alexander–de Gennes model[1-3] for the interaction between uncharged brushes. It allows one to express the total repulsion between two brushes as a combination of an increased osmotic force and a decreased elastic force, leading to eq 1. The local electroneutrality condition permits us to use a slightly modified form of this expression for our charged system. In contrast with eq 1, we used the Gaussian expression

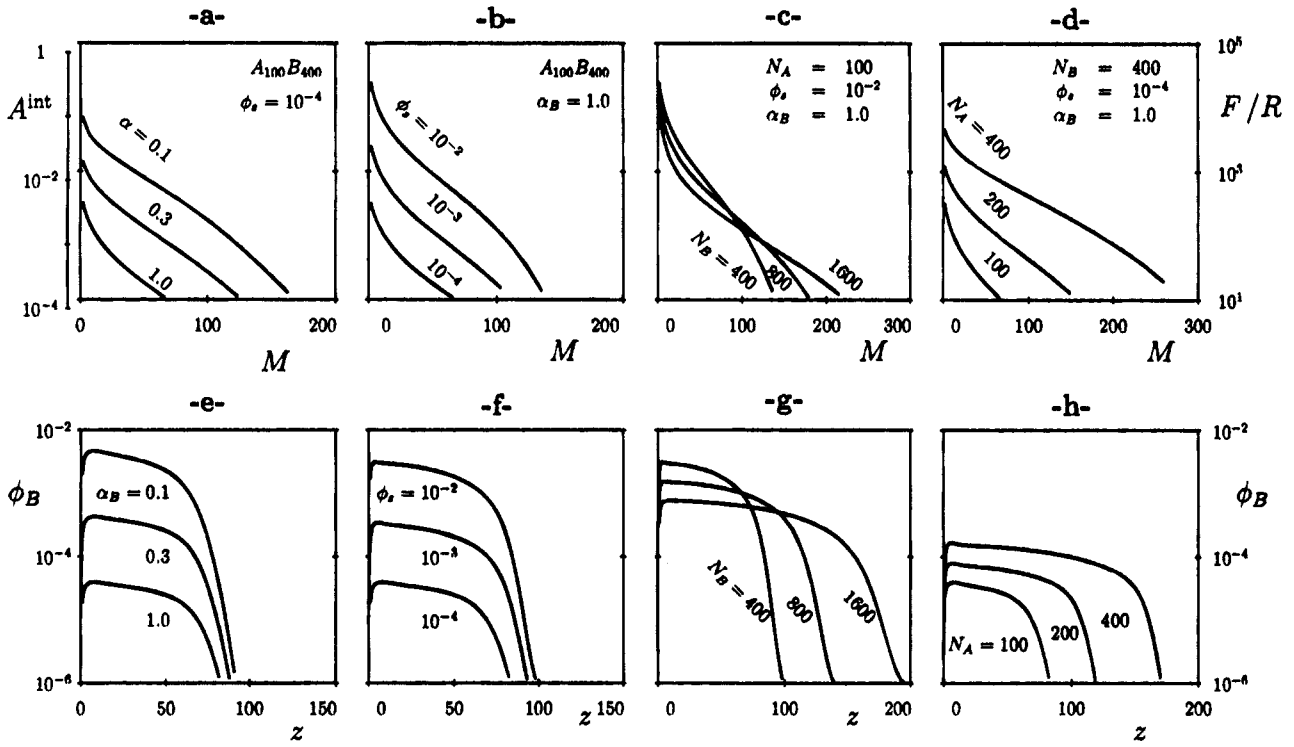

Figure 5. Interaction curves for different parameters as indicated (top row) and corresponding volume fraction profiles of the B units (bottom row). From left to right the effect of charge density (a,e), salt concentration (b,f), buoy block length (c,g), and anchor block length (d,h) is considered. Both the interaction curves and the density profiles are plotted on a log–lin scale. The interaction energy, which is calculated for the restricted case, is expressed in units of kT per site (left-hand scale). The right-hand scale gives the force-over-radius in μN/m, as obtained from the Deryaguin approximation.[23]

for the chain elasticity; for the osmotic force we applied the expression derived for the SB regime[10] to arrive at eq 25. Below we compare this analytical, but approximate, expression with mean-field calculations for various conditions.

Relation between Segment Density Profiles and Interaction Curves. In Figure 5 we have collected interaction curves and volume fraction profiles for a variety of systems, all of them located in the LC regime, for restricted equilibrium conditions. In the four upper frames (a–d), interaction curves are displayed on a log–lin scale. The left-hand scale gives the free energy of interaction in units of kT per lattice site (eq 21), as in Figure 3. This may be converted to a force between two curved surfaces using the Deryaguin approximation,[23] which leads to a "force-over-radius" value, expressed in μN/m, as used for the right-hand scale. Thus, the terms "interaction curve" and "force profile" have an identical meaning with respect to Figure 5; in the remainder of this text we will use both terms. Segment density profiles for the corresponding isolated brushes are presented in the four bottom figures (e–h), again on a log–lin scale. Each of the four bottom figures corresponds to its top counterpart: we consider the effect of the buoy block charge density α in Figure 5a,e, of the salt concentration ϕ_s in Figure 5b,f, of the buoy block length N_B in Figure 5c,g, and of the anchor block length N_A in Figure 5d,h.

Corresponding curves in the top and bottom figures were calculated using the same value for the adsorbed amount. The actual value we chose is the equilibrium adsorbed amount for isolated particles. This choice is debatable, since block copolymer adsorption is often not an equilibrium process; adsorbed amounts tend to depend heavily on the actual method of preparation. However, we wish to study the effect that system parameters have on this adsorbed amount. The only consistent choice, or best educated guess, we can make with our model is the equilibrium adsorbed amount. The assumption is that when a certain parameter causes a 10-fold decrease of this equilibrium adsorbed amount, the actual adsorbed amount will probably decrease also, whatever its method of preparation may be.

As explained in section III, the central part of the force profile is roughly exponential. Two features of this exponential part may be distinguished: the offset, which is determined by the prefactor in eq 25, and the slope, which is inversely proportional to the thickness H of an isolated adsorbed layer.

We start with discussing the effect of the charge density α on the buoy block. As shown in Figure 5e, and as discussed before,[16] an increase of the charge density leads to a decreased segment density in the brush, while its thickness remains the same. We would expect also the force profile in Figure 5a to reflect this constant thickness. At first sight this does not seem to be the case. However, as mentioned above, the constancy of the brush thickness should be reflected in a constant *slope* of the exponential part of the force profile on a log–lin plot, its offset decreasing with (2 log α). This is indeed what we see in Figure 5a.

According to eq 2, electrostatic effects can be accounted for in terms of an effective excluded volume parameter $v_{eff} = v + \alpha^2/4\phi_s$. Thus we expect the effect of the salt concentration ϕ_s, displayed in Figure 5b,f, to be opposite to that of the charge density α, discussed above. The brush density should increase linearly with the salt concentration (while the thickness remains constant again), resulting in an upward shift of the force profile. This expectation is quantitatively corroborated: a 10-fold *increase* in the charge density α has roughly the same effect as a 100-fold *decrease* in the salt concentration ϕ_s. The slightly higher repulsion at low separations for the upper interaction curve in Figure

5b as compared to the upper one in Figure 5a must be attributed to the effect of the volume of salt ions, which is neglected in the scaling analysis.

Variation of the block lengths N_A or N_B leads to a slightly more complex behavior, due to the fact that these parameters *do* have an effect on the thickness H. A higher anchor block length causes the density as well as the thickness of the adsorbed layer to increase (Figure 5h), the latter scaling with the square root of the block length. Increasing the buoy block length also leads to a more extended layer, which is accompanied, however, by a diminished density (Figure 5g).

As mentioned above, the slope of the exponential part in the force profile should be inversely proportional to the thickness H. This is indeed confirmed by Figure 5c,d: the 2-fold increase in H observed in either Figure 5g (going from $N_B = 400$ to 1600) or Figure 5h (going from $N_A = 100$ to 400) leads to a roughly two times lower slope in the force profiles 5c and 5d, respectively.

The variation of the magnitude of the interaction is more interesting. From the prefactor of eq 25 we read that the repulsive interaction increases with N_A and decreases with N_B. This effect is explained from the increasing and decreasing density resulting from making these blocks longer. Again, the agreement is semiquantitative: the effect of doubling the anchor block length, which increases N_A^3 by a factor of 8, is comparable to that of a 10-fold increase in the salt concentration. The effect of the buoy block length, on the other hand, is opposite and much weaker.

The trends found for the effects of N_A and N_B are easy to understand once the density profiles are known but would perhaps be less trivially explained in the absence of this information. For example, increasing the B tail does not automatically increase stability, as one might have guessed intuitively.

In the above we presented both segment density profiles and interaction curves. The density profiles are very dilute, as anticipated. Nevertheless, the magnitude of the force is well within the range that can be measured by the surface force apparatus. Another point of discussion is whether or not the interaction force can induce colloidal stability. In general, this will depend on the particle size. The total energy of interaction between two particles should exceed their average kinetic energy which is independent of the particle size and of order kT. Moreover, also the attractive van der Waals interaction should be compensated for. At least some of the interaction energies presented in Figure 5 are, for not too small particles, high enough to ensure stability. On the other hand, the calculations show clearly that the repulsive interactions approach zero when the electrostatic interactions become too strong (high α, low ϕ_s).

The exact point where a system begins to flocculate cannot be predicted with our model, since neither the particle entropy nor the van der Waals attraction is taken into account. Nevertheless, we do predict how stability is affected by the four parameters we investigated, as given by the prefactor in eq 25. We wish to stress that the result is counterintuitive: although the stability arises primarily from electrostatic interactions, any increase in the relative importance of those interactions (i.e., either increasing N_B/N_A^3 or α^2/ϕ_s) leads to a *lower* stability. As shown above, this is explained by the lower adsorbed amounts resulting from stronger electrostatic interactions.

The above result is valid for the LC regime, where the density of the adsorbed layer is determined by a balance of adsorption and electrostatic forces. We will try to place it in a broader perspective by examining the other regime that is relevant for this type of polymers: the anchor-dominated regime.[24] In the latter regime, found for high anchor block lengths, the density σ is unaffected by electrostatic forces and depends only on the anchor length N_A:

$$\sigma = 1/N_A \tag{26}$$

Our limited computer power prohibits numerical SCF calculations at the extremely high chain lengths required to investigate this regime. It seems obvious, however, to surmise that a higher charge on the buoy block must have a stabilizing effect in the anchor-dominated regime. This stabilizing effect would be expected in the LC regime also, but there it is more than offset by the effect this charging has on the adsorbed amount. Since stability increases with increasing electrostatic interactions in one regime and decreases in the other, a maximum must be found at the boundary between the two. An expression for the location of this boundary is found by equating the expressions for σ in the two regimes, eqs 23 and 26:

$$\phi_s^{max} = \alpha^2 N_B^{3/2} N_A^{-5/2} \tag{27}$$

We substitute this expression for ϕ_s^{max} in eq 25, to arrive at the following expression for the maximum repulsion:

$$A(M)^{maxint} = (N_A N_B)^{1/2}(1/M - 1/2H) \tag{28}$$

which leads to the speculation that the maximum stability that may be obtained with (charged) anchor–buoy diblock copolymers scales with the geometric mean of both block lengths. It would be interesting to check this prediction experimentally.

V. Conclusion

Using an SCF model, we calculated the interaction between two surfaces covered with an adsorbed layer of charged diblock copolymers. At low salt concentration and/or high charge density on the buoy block, the adsorbed amount for these molecules is very low. The calculations show, however, that despite this low adsorbed amount the repulsive interaction should be measurable with a surface force apparatus.

Although the van der Waals attraction is strong at short separations, it falls off very rapidly. Therefore, the calculated repulsive interaction might induce at least kinetic stability. We estimate that it may be strong enough to do so, provided the radius of the particles is sufficiently large.

We investigated the effect of the anchor block length N_A, of the length N_B of the charged buoy block, of the charge density α on this buoy block, and of the salt concentration ϕ_s on the strength of the repulsion. Intuitively, one might expect the repulsion to increase when electrostatic interactions become more important. However, we show the effect to be exactly opposite in a large part or the parameter space. Specifically, when the adsorption is low and the charge high, the repulsive interaction scales as $N_A^3\phi_s/N_B\alpha^2$. This is attributed to the fact that increasing electrostatic interactions lead to a decreased adsorbed amount.

Finally, we argue that such a charge-induced desorption does not occur in the so-called anchor-dominated regime. This leads us to speculate that the crossover between the anchor-dominated and low-coverage regimes is the location of maximum colloidal stability. We calculate the repulsive interaction at this maximum to scale with the geometric mean of *both* block lengths.

References and Notes

(1) Alexander, S. J. *J. Phys. (Paris)* **1977**, *38*, 983.
(2) de Gennes, P.-G. *C. R. Acad. Sci. (Paris)* **1985**, *300*, 839.
(3) de Gennes, P.-G. *Adv. Colloid Interface Sci.* **1987**, *27*, 189.
(4) Evers, O. A.; Scheutjens, J. M. H. M.; Fleer, G. J. *Macromolecules* **1991**, *24*, 5558.
(5) Pincus, P. *Macromolecules* **1991**, *24*, 2912.
(6) Borisov, O. V.; Birshtein, T. M.; Zhulina, E. B. *J. Phys. II* **1991**, *1*, 521.
(7) Borisov, O. V.; Priamitsin, V. A.; Birshtein, T. M. *Macromolecules* **1991**, *24*, 140.
(8) Zhulina, E. B.; Borisov, O. V.; Priamitsin, V. A. *J. Colloid Interface Sci.* **1990**, *137*, 495.
(9) Zhulina, E. B.; Borisov, O. V.; Priamitsin, V. A.; Birshtein, T. M. *Macromolecules* **1991**, *24*, 140.
(10) Zhulina, E. B.; Birshtein, T. M.; Borisov, O. V. *J. Phys. II* **1992**, *2*, 63.
(11) Israëls, R.; Leermakers, F. A. M.; Fleer, G. J.; Zhulina, E. B. *Macromolecules* **1994**, *27*, 3249.
(12) Milner, S. T.; Witten, T. A.; Cates, M. E. *Macromolecules* **1988**, *21*, 1366.
(13) Argillier, J. F.; Tirrell, M. *Theor. Chim. Acta* **1992**, *82*, 343.
(14) Wittmer, J.; Joanny, J.-F. *Macromolecules* **1993**, *26*, 2691.
(15) Marques, C. M.; Joanny, J.-F.; Leibler, L. *Macromolecules* **1988**, *21*, 1051.
(16) Israëls, R.; Scheutjens, J. M. H. M.; Fleer, G. J. *Macromolecules* **1993**, *26*, 5404.
(17) Evers, O. A.; Scheutjens, J. M. H. M.; Fleer, G. J. *J. Chem. Soc., Faraday Trans.* **1990**, *86*, 1333.
(18) Böhmer, M. R.; Evers, O. A.; Scheutjens, J. M. H. M. *Macromolecules* **1990**, *23*, 2288.
(19) Fleer, G. J.; Cohen Stuart, M. A.; Scheutjens, J. M. H. M.; Cosgrove, T.; Vincent, B. *Polymers at Interfaces*; Chapman & Hall: London, 1993.
(20) Lent, B. van; Scheutjens, J. M. H. M. *Macromolecules* **1989**, *22*, 1931.
(21) Shull, K. *Macromolecules* **1993**, *26*, 2346.
(22) de Gennes, P.-G. *J. Phys. (Paris)* **1976**, *37*, 1461.
(23) Deryaguin, B. V. *Kolloid Z.* **1934**, *69*, 155.
(24) Marques, C. M.; Joanny, J.-F. *Macromolecules* **1989**, *22*, 1454.
(25) See, e.g.: Israelachvili, J. *Intermolecular and Surface Forces*, 2nd ed.; Academic Press: New York, 1991.

MA941263E